

---

# Integrative Feature and Cost Aggregation with Transformers for Dense Correspondence

---

Sunghwan Hong\*  
Korea University

Seokju Cho\*  
Korea University

Seungryong Kim†  
Korea University

Stephen Lin  
Microsoft Research Asia

## Abstract

We present a novel architecture for dense correspondence. The current state-of-the-art are Transformer-based approaches that focus on either feature descriptors or cost volume aggregation. However, they generally aggregate one or the other but not both, though joint aggregation would boost each other by providing information that one has but other lacks, *i.e.*, structural or semantic information of an image, or pixel-wise matching similarity. In this work, we propose a novel Transformer-based network that interleaves both forms of aggregations in a way that exploits their complementary information. Specifically, we design a self-attention layer that leverages the descriptor to disambiguate the noisy cost volume and that also utilizes the cost volume to aggregate features in a manner that promotes accurate matching. A subsequent cross-attention layer performs further aggregation conditioned on the descriptors of both images and aided by the aggregated outputs of earlier layers. We further boost the performance with hierarchical processing, in which coarser level aggregations guide those at finer levels. We evaluate the effectiveness of the proposed method on dense matching tasks and achieve state-of-the-art performance on all the major benchmarks. Extensive ablation studies are also provided to validate our design choices.

## 1 Introduction

Finding visual correspondence between images is a central problem in computer vision, with numerous applications including simultaneous localization and mapping (SLAM) [3], augmented reality (AR) [53], object tracking, structure from motion (SfM) [62], optical flow [18], and image editing [5, 34]. Given visually or semantically similar images, unlike sparse correspondence approaches [43, 7, 79, 13, 51, 16, 55] that first detect a set of sparse points and extract corresponding descriptors to find matches across them, dense correspondence [71, 25, 82, 28] aims at finding matches for all pixels. Dense correspondence approaches typically follow the classical matching pipeline [61, 54] of feature extraction, cost aggregation, and flow estimation.

Much research has designed a means to address either the feature extraction or the cost aggregation, as shown in Fig. 1 (a) and (b). Feature aggregation aims to not only integrate self-similar features within an image and but also align similar features between the two images for matching, such as by using deep dense feature descriptors [36, 60, 68, 77, 32]. The advantages of feature aggregation are particularly evident in attention and Transformer-based methods [74, 60, 68, 32, 77] thanks to their attention layers with global receptive fields and adaptability to input tokens, which previous works with convolutions [59, 36, 31, 25, 46] lack. These methods, however, solely aggregate feature descriptors without consideration of cost aggregation. Numerous works [59, 27, 37, 40, 60, 46, 47, 9, 68, 23, 28, 10] on dense correspondence proposed methods for cost aggregation stage instead and demonstrate its importance. During cost aggregation, pair-wise interactions between pixels of the two

---

\*Equal contribution

†Corresponding author

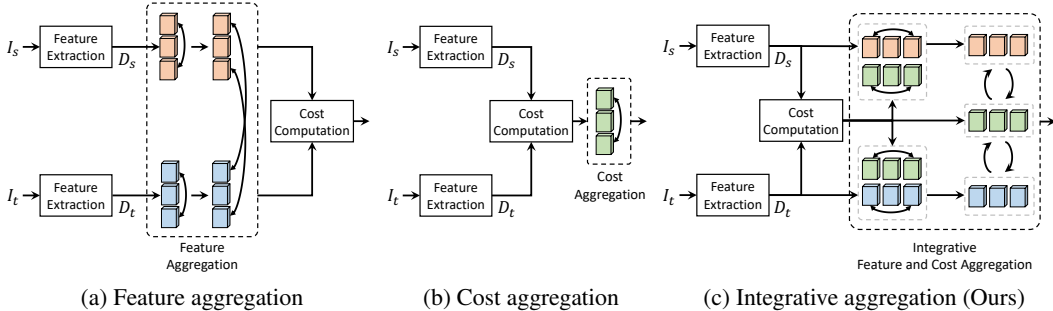


Figure 1: **Intuition of the proposed method:** (a) feature aggregation methods [68, 77, 32] that aggregate feature descriptors, (b) cost aggregation methods [9, 28] that aggregate a cost volume, and (c) our integrative feature and cost aggregation method, which jointly performs both aggregations in a complementary manner.

images are considered by first computing a cost volume between descriptors and then suppressing noise to promote accurate correspondence estimation. Transformer-based methods [9, 28] are found to benefit significantly from cost aggregation, but they disregard aggregation of feature descriptors even though an improved cost volume constructed using less noisy features would ease the subsequent cost aggregation.

We argue that both feature aggregation and cost aggregation should ideally be performed in dense correspondence, as they serve different purposes and the benefits of each are well-established. Although there have been a few approaches [60, 25] that attempt to aggregate both, no approaches utilized transformers due to its expensive computational complexity, and we believe that directly performing the two aggregations independently in a sequential manner only allows one aggregation to benefit the other but not vice versa, thus limiting the synergy between these two processes.

In this work, we present a method, which we call **Integrative Feature and Cost Aggregation with Transformers (IFCAT)**, that jointly aggregates feature descriptors and the cost volume in a manner that leverages their complementarity, as shown in Fig. 1 (c). This goal is accomplished in two steps, the first of which employs a self-attention layer to jointly aggregate the descriptors and cost volume. In this stage, the descriptors help to disambiguate the noisy cost volume similarly to cost volume filtering [26, 67], and the cost volume enhances feature aggregation by introducing matching similarities as a factor for aggregation. The cost volume explicitly represents the similarity of features in one image with respect to the features in the other, and accounting for it drives the features in each image to become more compatible with those of the other. In the subsequent step, we design a cross-attention layer that performs further aggregation aided by both the feature descriptors and the cost volume from earlier aggregations. By constructing better cross-attention maps with both the feature descriptors and the aggregated cost volume, the aggregated features of both images can be mutually improved more effectively. These self- and cross-attention layers are interleaved to facilitate convergence. We further boost performance through hierarchical processing that enhances this complementary aggregation by providing coarser outputs to guide finer-level aggregation.

We evaluate the proposed method on semantic and geometric matching tasks. In the experiments, we show that IFCAT outperforms prior works on all the major benchmarks, including SPair-71k [49], PF-PASCAL [20], PF-WILLOW [19] and HPatches [4], by a significant margin, establishing a new state-of-the-art for all of them. We also conduct an extensive ablation study to validate our approach and the architectural design choices. The pre-trained weights and codes will be made available.

## 2 Related Work

**Feature Extraction.** Various methods have been proposed to extract feature descriptors for robust sparse matching. This process involves detecting interest points and extracting the descriptors of corresponding points. In traditional methods [39, 6, 11, 69], the matching performance mostly relies on the quality of the feature detection and the description method, and outlier rejection across matched points is typically determined by RANSAC [17]. These methods focus on the problem of identifying

more meaningful feature points and extracting feature descriptors given an image. Despite their solid performance, they often struggle in cases of extreme appearance or viewpoint changes.

To overcome such issues, several methods [79, 13, 51, 16, 55] extract dense deep features used to obtain descriptors tailored for matching. These works have demonstrated that the quality of feature descriptors contributes substantially to matching performance. In accordance with this, recent matching networks [13, 60, 48, 36, 25, 50, 32, 68, 77] proposed effective means for feature aggregation. Notable works include SuperGlue [60], which employs graph self- and cross-attention to aggregate deep feature maps. SFNet [36] and DMP [25] introduce an adaptation layer subsequent to feature extraction in order to learn feature maps well-suited to matching.

Recent state-of-the-art works utilize Transformer [74] for feature aggregation. COTR [32] uses transformers by taking input coordinates and feature maps to infer the correspondence of a given pixel coordinate, with self-attention computed for feature aggregation. LOFTR [68] also uses self- and cross-attention, but leaves the cost aggregation to a handcrafted method, *i.e.*, optimal transport [66]. Very recently, GMFlow [77] also utilized a transformer for feature aggregation in optical flow estimation. Despite its state-of-the-art performance, its disregard of cost aggregation may lead to sub-optimal solutions, a problem we address in this paper.

**Cost Aggregation.** In the correspondence literature, recent works carefully design their architecture to effectively aggregate a cost volume. Some works [15, 67, 29, 45, 71, 25, 31, 72] use 2D convolutions to establish correspondence while aggregating the cost volume with learnable kernels that have a local receptive field. Although 2D convolutions are used for flow estimation, they in fact also aggregate costs during the process, making them suitable for both the cost aggregation and flow estimation stages. Some works [48, 50, 40] utilize handcrafted methods including RHM [8] and the OT solver [66]. These works have inherent limitations as their use of handcrafted techniques do not take advantage of learning and are susceptible to severe deformations. NC-Net [59] proposes to use 4D convolutions for cost aggregation in order to identify sets of consistent matches by exploring neighborhood consensus. Inspired by this, numerous works [37, 78, 27, 58, 46, 47] either adopted or extended 4D convolutions. For example, DCCNet [27] used it for cost embedding; Sparse NC-Net [37] designed adaptive 4D convolutions, and [78, 58, 47] proposed efficient versions. However, they are all limited in the sense that they inherit the limitations of CNN-based architectures, for which the receptive fields are local.

Recently, CATs [9] proposed to use Transformer [74] as a means for cost aggregation, and an extension [10] combined convolutions with Transformer for enhanced cost aggregation. Although they benefit from the global receptive field of self-attention operations, they disregard feature aggregation even though the cost volume they use is constructed from feature maps. FlowFormer [28] takes an approach that utilizes Transformer, but it is designed specifically for the optical flow task and does not aggregate features. By disregarding feature aggregation, these methods may limit their performance due to the resultant noise in the cost volume which then hampers cost aggregation.

### 3 Preliminaries: Self- and Cross-Attention

Self- and cross-attention are the core elements of Transformer [74] for their ability to globally model relationships and interactions among input tokens and their adaptability to input tokens. As a general description, given a sequence of tokens as an input, Transformer [74] first linearly projects tokens to obtain query, key and value embeddings. These are then fed into a scaled dot product attention layer, followed by layer normalization (LN) [1] and a feed-forward network or MLP, to produce an output with the same shape as the input. Each token is attended to by all the other tokens. This attention process can be formulated as:

$$Q = \mathcal{P}_Q(X), \quad K = \mathcal{P}_K(X), \quad V = \mathcal{P}_V(X), \quad (1)$$

where  $\mathcal{P}_Q$ ,  $\mathcal{P}_K$  and  $\mathcal{P}_V$  denote query, key and value projections, respectively, and  $X$  denotes a token with a positional embedding. The obtained query, key and value embeddings then pass through an attention layer:

$$\text{Attention}(X) = \text{softmax}\left(\frac{QK^T}{\sqrt{d_k}}\right)V, \quad (2)$$

where  $d_k$  is the dimension of key embeddings. Note that the  $\text{Attention}(\cdot)$  function can be defined in various ways [75, 41, 33, 44, 76]. A key factor that distinguishes self- and cross-attention is the

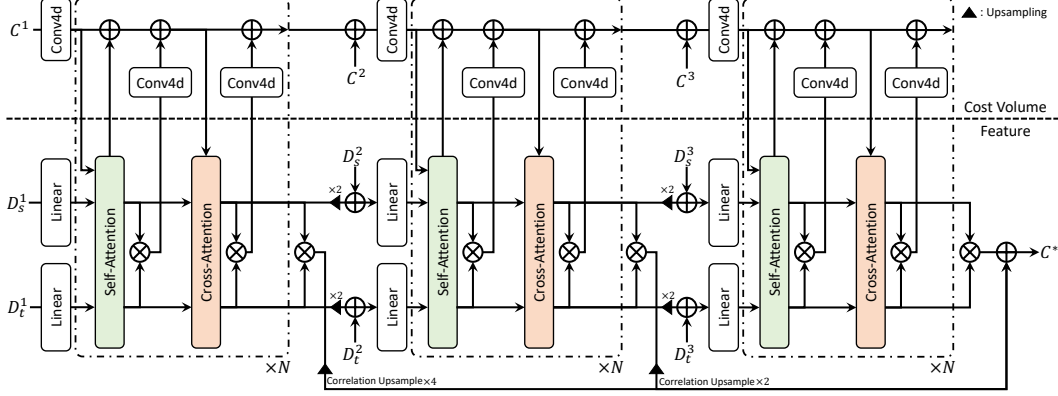


Figure 2: **Overall architecture of the proposed method.** Given feature maps  $D_s$  and  $D_t$ , and cost volume  $C$  as inputs, our method employs self- and cross-attention specifically designed to conduct joint feature aggregation and cost aggregation in a coarse-to-fine manner.

input to the key and value projections. Given a pair of input tokens, e.g.,  $X_s$  and  $X_t$ , the input to the key and value projections when performing self-attention with  $X_s$  is the same input,  $X_s$ , but for cross-attention across  $X_s$  and  $X_t$ , the inputs to the key and value projection are  $X_t$ .

## 4 Methodology

### 4.1 Problem Formulation

Let us denote a pair of visually or semantically similar images, i.e., the source and target, as  $I_s$  and  $I_t$ , the feature descriptors extracted from  $I_s$  and  $I_t$  as  $D_s$  and  $D_t$ , respectively, and the cost volume computed between the feature maps as  $C$ . Given  $I_s$  and  $I_t$ , we aim to establish a correspondence field  $F(i)$  that is defined at all pixels  $i$  and warps  $I_s$  towards  $I_t$ .

Recent learning-based networks [56, 59, 58, 9] accomplish dense correspondence by extracting features from deep CNNs [22] or Transformers [14] for  $D_s$  and  $D_t$ . The extracted features subsequently undergo  $l_2$  normalization. A cost volume that consists of all pair-wise feature similarities  $C \in \mathbb{R}^{h \times w \times h \times w}$  with height  $h$  and width  $w$  is then computed and stored:  $C(i, j) = D_s(i) \cdot D_t(j)$ , where  $i$  and  $j$  index the source and target features, respectively. To improve the matching performance, existing state-of-the-art methods perform either feature aggregation [68, 77] or cost aggregation [9, 28] with Transformer [74] such that  $\{D'_s, D'_t\} = \mathcal{T}(D_s, D_t)$  or  $C' = \mathcal{T}(C)$ , where  $\mathcal{T}(\cdot)$  denotes Transformer. Then,  $F(i)$  is determined from  $C'(i, j)$  considering all  $j$ .

### 4.2 Motivation and Overview

We argue that solely focusing on either feature or cost aggregation may lead to sub-optimal solutions. While feature aggregation [68, 77] is a process of aligning similar features based on the rich structural or semantic information present in dense feature maps, cost aggregation [28, 9] is a process of suppressing noises based on matching similarities. The information the two aggregations consider are different, but they can enhance matching by improving each other's aggregation with the help of information that the other has.

In this work, we aim to jointly learn feature and cost aggregation modules by establishing a complementary relationship between them. To this end, we first concatenate a cost volume and feature descriptors, which we call a feature cost volume, and feed it to the self-attention layer. Within the self-attention layer, both feature and cost aggregation are performed, where the feature descriptors and the cost volume benefit from one another during the aggregation. Subsequently, we leverage the aggregated features and cost volume for cross-attention, which performs further aggregation aided by the aggregated inputs to the cross-attention layer. These self- and cross-attention layers are interleaved to facilitate convergence. Finally, we formulate our architecture in a coarse-to-fine manner, where the outputs of coarser attention blocks are used to guide the aggregation of finer-level blocks. In the following, we will explain each module in detail.

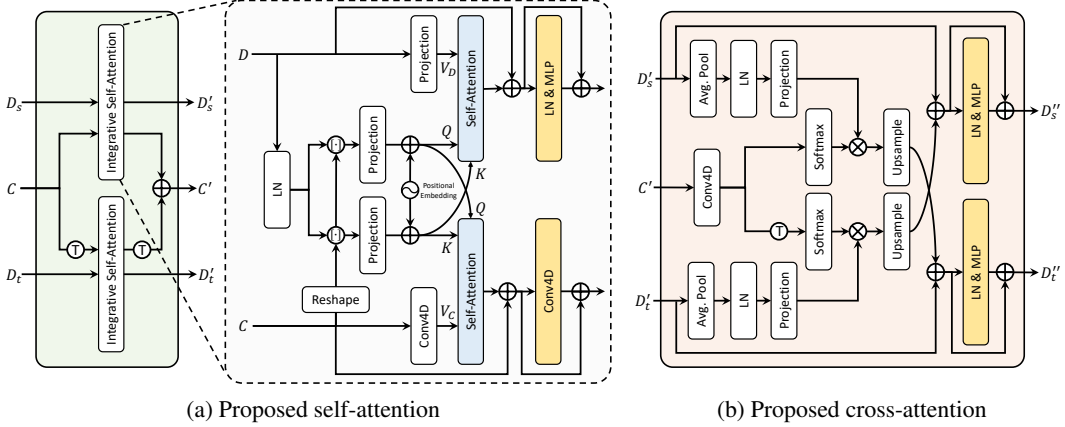


Figure 3: **Illustration of the proposed self- and cross-attention:** (a) self-attention layer that performs joint feature aggregation and cost aggregation, and (b) cross-attention layer with matching distribution for enhanced feature aggregation.

### 4.3 Integrative Feature and Cost Aggregation

**Self-Attention for Integrative Feature and Cost Aggregation.** Subsequent to feature extraction and cost computation, we feed both feature descriptors  $D_s$ ,  $D_t$  and cost volume  $C$  into our proposed self-attention layer. We first embed these inputs with linear projection for channel reduction prior to self-attention, and positional embeddings [74] are added after the query and key projections, as shown in Fig. 2. As done in [59], to ensure input order invariance, we consider the bidirectional nature of cost volumes and feed a pair  $\{D_s, C\}$  and  $\{D_t, C^T\}$  into the proposed self-attention layer independently, where  $C^T(i, j) = C(j, i)$ , and add the outputs.

Specifically, as shown in Fig. 3, within the self-attention layer, we first obtain a feature cost volume  $[D, C]$  by concatenating  $D$  and  $C$ , where  $[\cdot]$  denotes concatenation. To compute self-attention, we need to define the query, key and value embeddings. Unlike other works [68, 9] that solely aggregate either the feature descriptors or cost volume, we jointly aggregate both. To this end, we exploit the feature cost volume in computing self-attention and define two independent value embeddings, specifically one for feature projection and the other for cost volume projection. Note that we do not use the feature cost volume for value embeddings to ensure disentangled aggregation that is targeted for one and not the other. Formally, we define the query, key and values as:

$$Q = \mathcal{P}_Q([D, C]), \quad K = \mathcal{P}_K([D, C]), \quad V_D = \mathcal{P}_{V_D}(D), \quad V_C = \mathcal{P}_{V_C}(C), \quad (3)$$

where  $V_D$  and  $V_C$  denote the value embeddings of feature descriptors and the cost volume, respectively. After computing an attention map by applying softmax over the query and key dot product, we use it to aggregate feature  $D$  and cost volume  $C$  with  $V_D$  and  $V_C$  using Eq. 2 as follows:

$$\text{Attention}_{\text{self-D}}(C, D) = \text{softmax}\left(\frac{QK^T}{\sqrt{d_k}}\right)V_D, \quad \text{Attention}_{\text{self-C}}(C, D) = \text{softmax}\left(\frac{QK^T}{\sqrt{d_k}}\right)V_C. \quad (4)$$

Note that any type of attention computation can be utilized, *i.e.*, additive [2] or dot product [74], while in practice we use the linear kernel dot product with the associative property of matrix products [33]. The outputs of this self-attention are denoted as  $D'_s$ ,  $D'_t$ , and  $C'$ .

In this way, we benefit from two perspectives. From the cost aggregation point of view, the feature map of the feature cost volume can disambiguate the noisy cost volume as proven in the stereo matching literature [80, 26, 21], *i.e.*, cost volume filtering, which aids the cost aggregation process. From the feature aggregation point of view, the cost volume explicitly represents the similarity of features in one image with respect to the features in the other, and accounting for it drives the features in each image to become more compatible with those of the other.

**Cross-Attention with Matching Distribution.** In the proposed cross-attention layer, the aggregated feature and cost volume are explicitly used for further aggregation, and we condition both feature descriptors on both input images via this layer. By exploiting the outputs of the self-attention

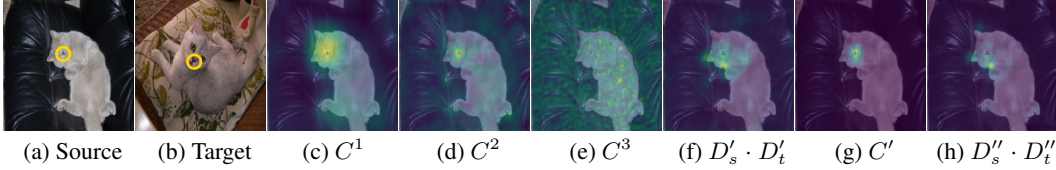


Figure 4: **Visualization of attention maps:** (a) source image, (b) target image, (c)-(e) raw correlations, (f) a cost volume constructed with features aggregated with self-attention, (g) a cost volume aggregated with self-attention, and (h) a cost volume constructed with features aggregated with cross-attention.

layer, the cross-attention layer performs cross-attention between feature descriptors for further feature aggregation using the improved feature descriptors  $D'_s$ ,  $D'_t$  and enhanced cost volume  $C'$  from earlier aggregations.

Concretely, as shown in Fig. 3, we first treat the input cost volume as a cross-attention map, since applying a softmax function over the cost volume is tantamount to obtaining an attention map. In this way, we could perform more enhanced aggregation as the input cost map to the cross-attention layer is guided by residual connections that contain information from improved features and an enhanced cost volume as further explained in the next paragraph. Note that features  $D'_s$  and  $D'_t$  undergo average pooling followed by layer normalization [1] and a linear projection layer in order to adjust the spatial resolution to  $C'$ , as will be further explained in Section 4.4. Formally, we first define a cross-attention map and value for attention score as  $QK^T = C'$  and  $V_{D'} = \mathcal{P}_{V_D}(D')$ , respectively. The attention process for cross-attention is then defined as follows:

$$\text{Attention}_{\text{cross}}(C', D') = \text{softmax}\left(\frac{C'}{\sqrt{d_k}}\right)V_{D'}. \quad (5)$$

The outputs of this cross-attention are denoted as  $D''_s$ ,  $D''_t$ , and  $C''$ .

**Enhanced Aggregation with Improved Features and Cost Volume.** Within the proposed attention block, it is shown in Fig. 2 that the outputs of the self- and cross-attention layers, which include aggregated feature maps and a cost volume, are connected to the next layer or added to the input cost volume. Specifically, the feature maps are used in two ways: for cost volume construction and as inputs to aggregation in subsequent layers. For cost volume construction, the aggregated features are processed according to Eq. 3 and the result is added to the cost volume input of the next layer by a residual connection. This is repeated for both self-attention and cross-attention layers across  $N$  attention blocks, where the aggregated pairs of one block are fed as input to the following attention block. Similar to the feature maps, the cost volume is progressively improved from aggregation and better features as it passes through the attention blocks. Through these mechanisms of the proposed joint aggregation, the feature maps and cost volume help each other in self-attention and also facilitate further aggregation by providing an enhanced cross-attention map and improved features.

#### 4.4 Coarse-to-Fine Formulation

To improve the robustness of fine-scale estimates, we extend our architecture to a coarse-to-fine approach through pyramidal processing, as done in [30, 45, 71, 25]. Specifically, we use feature maps of the last index at each pyramid level, specifically feature maps from conv $3_x$  to conv $5_x$  when ResNet [22] is used. We first use a coarse pair of refined feature maps and aggregated cost volume, and similar to [81] that learns complementary correspondence by adding the cost volume of the previous scale, we progressively learn complementary descriptors and correspondences through adding the previous-level outputs to those of the next level.

The overall architecture is shown in Fig. 2. A straightforward solution would be to upsample all the outputs of the cross-attention layer, following a pyramidal structure. However, the increasing computational and memory burden with respect to the cost volume resolution makes this infeasible. To alleviate such issues, we fix the resolution of the cost volume to the coarsest resolution and utilize 4D convolutions to downsample the spatial resolution when finer cost volumes are added to the coarsest cost volume. Finally, we sum up the output cost volumes after each attention block computed using the enhanced feature maps across all levels for the final output of the network. Formally, given the outputs of the attention block at each level,  $D''_s{}^l$ ,  $D''_t{}^l$  and  $C''^l$ , where  $l$  denotes the  $l$ -th level,

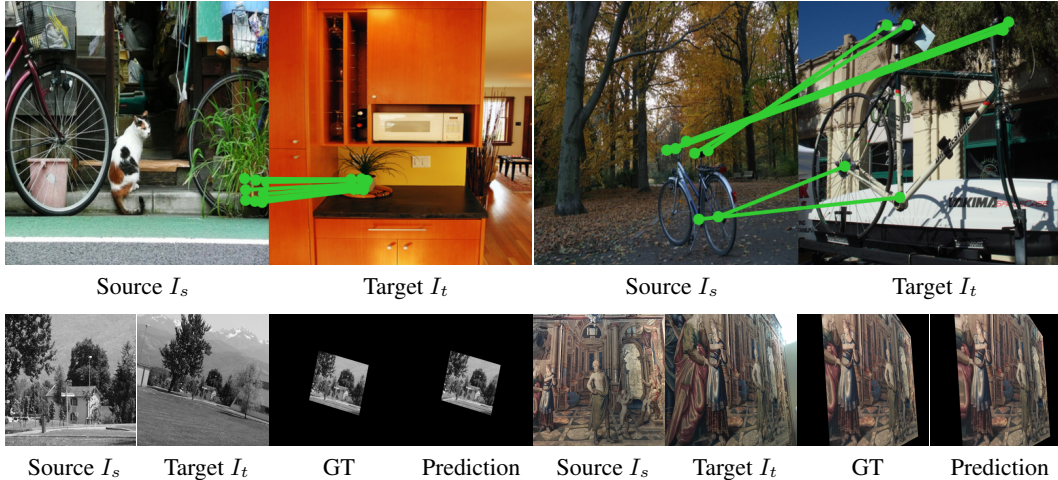


Figure 5: **Qualitative results on SPair-71k [49] (top) and HPatches [4] (bottom).**

we upsample the aggregated features using bilinear interpolation, and add them to the raw feature descriptors extracted from  $I_s$  and  $I_t$  defined at the next level:  $D_s^{l+1} = D_s^{l+1} + \text{up}(D_s^{\prime,l})$ , where  $D_t^{l+1}$  is defined similarly. In addition,  $C^{l+1} = C^{l+1} + \text{Conv4d}(C^{\prime\prime,l})$ . The visualizations of cost volumes are shown in Fig. 4.

Finally, given the features  $D_s^{\prime\prime}$  and  $D_t^{\prime\prime}$  at each level, we compute the correlation map between  $D_s^{\prime\prime}$  and  $D_t^{\prime\prime}$ , and the sum of cost volumes across all levels are added up to obtain the final output  $C^*$  that is used to estimate the final flow field, as shown in the bottom of Fig. 2.

#### 4.5 Training Objective

To train the networks, we first compute the correlation map between  $D_s^{\prime\prime}$  and  $D_t^{\prime\prime}$  at each level and then transform it into a dense flow field  $F_{\text{pred}}$  using the soft-argmax operator [36]. Then, we compare the predicted dense flow field with the ground-truth flow field  $F_{\text{GT}}$ . Specifically, we use average end-point error (AEPE), computed by averaging the Euclidean distance between the ground-truth and estimated flow, for the objective function. We then sum up the AEPE loss across all levels. We thus formulate the objective function as  $\mathcal{L} = \|F_{\text{GT}} - F_{\text{pred}}\|_2$ . Flow fields may instead be obtained from  $C^{\prime\prime}$ , but we empirically find that slightly better results are obtained when feature maps are used.

## 5 Experiments

### 5.1 Implementation Details

For the backbone network, we use VGG-16 [65] for dense alignment and ResNet-101 [22] for dense semantic correspondence, which are both pretrained on ImageNet [12]. We use  $N = (2, 2, 2)$  for efficiency in training. We use data augmentation used in [9] for dense semantic correspondence, while no augmentation is used for dense alignment. Our networks are trained with the input images resized to  $512 \times 512$ . We implemented our network using PyTorch [52], and the AdamW [42] optimizer is employed with an initial learning rate of  $1e-4$  for the IFCAT layers, which we gradually decrease using step learning rate decay. We train our networks for 50 epochs on SPair-71k [49] and DPED-CityScape-ADE [71], and 300 epochs for PF-PASCAL [20]. More details can be found in the supplementary material. The code and pretrained weights will be made publicly available.

### 5.2 Dense Semantic Correspondence

In this section, we evaluate the effectiveness of the proposed method for dense correspondence. For a fair comparison, following [34, 27, 48, 50, 9], when evaluating on SPair-71k [49] we train the proposed method on SPair-71k [49], and when evaluating on PF-PASCAL [20] and PF-WILLOW [19] we train on PF-PASCAL [20].

Table 1: **Quantitative evaluation on standard semantic correspondence benchmarks [49, 19, 20].** Higher PCK is better. The best results are in bold, and the second best results are underlined. *Reso.:* Resolution, *F.A.:* Feature Aggregation, *C.A.:* Cost Aggregation.

Methods	Reso.	F.A.	C.A.	SPair-71k [49]	PF-PASCAL [20]			PF-WILLOW [19]			
				PCK @ $\alpha_{\text{bbox}}$ 0.1	PCK @ $\alpha_{\text{img}}$ 0.05 0.1 0.15			PCK @ $\alpha_{\text{bbox}}$ 0.05 0.1		PCK @ $\alpha_{\text{bbox-kp}}$ 0.05 0.1	
CNNGeo [56]	Ori	-	2D Conv.	20.6	41.0	69.5	80.4	-	-	36.9	69.2
A2Net [63]	-	-	2D Conv.	22.3	42.8	70.8	83.3	-	-	36.3	68.8
WeakAlign [57]	Ori	-	2D Conv.	20.9	49.0	74.8	84.0	-	-	37.0	70.2
RTNs [34]	-	-	2D Conv.	25.7	55.2	75.9	85.2	-	-	41.3	71.9
SFNet [36]	288/Ori	2D Conv.	-	-	53.6	81.9	90.6	-	-	46.3	74.0
NC-Net [59]	240/ori/400	-	4D Conv.	20.1	54.3	78.9	86.0	-	-	33.8	67.0
DCC-Net [27]	240/ori/-	-	4D Conv.	-	55.6	82.3	90.5	-	-	43.6	73.8
HPF [48]	Max 300	-	RHM	28.2	60.1	84.8	92.7	-	-	45.9	74.4
GSF [31]	-	-	2D Conv.	36.1	65.6	87.8	95.9	-	-	<u>49.1</u>	<b>78.7</b>
ANC-Net [37]	-	-	4D Conv.	-	-	86.1	-	-	-	-	-
DHPF [50]	240	-	RHM	37.3	75.7	90.7	95.0	49.5	77.6	-	71.0
SCOT [40]	Max 300	-	OT-RHM	35.6	63.1	85.4	92.7	-	-	47.8	76.0
CHM [46]	240	-	6D Conv.	46.3	80.1	91.6	94.9	52.7	79.4	-	69.6
PMNC [35]	400	-	4D Conv.	50.4	<u>82.4</u>	90.6	-	-	-	-	-
CATs [9]	256	-	Trans.	49.9	75.4	<u>92.6</u>	<u>96.4</u>	50.3	79.2	40.7	69.0
MMNet-FCN [81]	224×320	Conv.+Trans.	-	50.4	81.1	91.6	95.9	-	-	-	-
PMD [38]	-	Attention	-	37.4	-	90.7	-	-	-	-	75.6
PWarpC-NC-Net [73]	Ori	-	4D Conv.	52.0	79.2	92.1	95.6	-	-	48.0	<u>76.2</u>
VAT [24]	512	-	Conv.+Trans.	<u>55.5</u>	78.2	92.3	96.2	<u>52.8</u>	<b>81.6</b>	-	-
<b>IFCAT (Ours)</b>	Ori	Trans.	Trans.	<b>64.4</b>	<b>88.0</b>	<b>94.8</b>	<b>97.9</b>	<b>58.6</b>	<u>81.2</u>	<b>50.4</b>	74.2

Table 2: **Quantitative evaluation on HPatches [4].** We evaluate on both HPatches-240 and HPatches original. Lower AEPE is better. We divide methods into two groups: multiple feed-forward and single feed-forward.

Methods	F.A.	C.A.	HPatches (240 × 240)						PCK	HPatches						PCK
			AEPE ↓							AEPE ↓						
			I	II	III	IV	V	Avg.		I	II	III	IV	V	Avg.	
COTR [32]	Trans.	<b>X</b>	-	-	-	-	-	-	-	-	-	-	-	-	7.75	<b>91.10</b>
RANSAC-Flow [64]	2D Conv.	<b>X</b>	<b>0.51</b>	2.36	2.91	<b>4.41</b>	<b>5.12</b>	3.06	-	-	-	-	-	-	-	-
RANSAC-DMP [25]	2D Conv.	2D Conv.	<u>0.53</u>	<b>2.21</b>	<b>2.76</b>	4.62	5.14	<b>3.05</b>	<b>96.28</b>	<b>4.32</b>	<b>11.21</b>	<b>22.80</b>	<b>31.34</b>	<b>33.64</b>	<u>20.65</u>	<b>75.35</b>
CNNGeo [56]	<b>X</b>	2D Conv.	9.59	18.55	21.15	27.83	35.19	22.46	-	-	-	-	-	-	-	-
DGC-Net [45]	<b>X</b>	2D Conv.	1.74	5.88	9.07	12.14	16.50	9.07	50.01	5.71	20.48	34.15	43.94	62.01	33.26	58.06
GLU-Net [71]	<b>X</b>	2D Conv.	<b>0.59</b>	<u>4.05</u>	<u>7.64</u>	<u>9.82</u>	<u>14.89</u>	<u>7.40</u>	<u>83.47</u>	<u>1.55</u>	12.66	27.54	32.04	52.47	25.05	78.54
GOCOR-GLU-Net [70]	<b>X</b>	Hand-crafted	-	-	-	-	-	-	-	<b>1.29</b>	<b>10.07</b>	<u>23.86</u>	<u>27.17</u>	<u>38.41</u>	<u>20.16</u>	<b>81.43</b>
DMP [25]	2D Conv.	2D Conv.	1.21	5.12	12.31	13.68	16.12	9.69	79.21	3.21	15.54	32.54	38.62	63.43	30.64	63.21
<b>IFCAT (Ours)</b>	Trans.	Trans.	<u>0.65</u>	<b>3.33</b>	<b>5.41</b>	<b>6.91</b>	<b>10.09</b>	5.27	<b>90.90</b>	1.90	<u>10.72</u>	<b>18.95</b>	<b>24.36</b>	<b>31.40</b>	<b>17.59</b>	<u>80.41</u>

SPair-71k [49] consists of 70,958 image pairs with extreme and diverse viewpoints, scale variations, and rich annotations for each image pair. PF-PASCAL [19] contains 1,351 image pairs over 20 object categories with keypoint annotations, and PF-WILLOW [19] is composed of 900 image pairs from 4 categories. We use percentage of correct keypoints (PCK) for the evaluation metric, for which higher values are better. Concretely, given predicted keypoint  $k_{\text{pred}}$  and ground-truth keypoint  $k_{\text{GT}}$ , we count the number of predicted keypoints that satisfy the following condition:  $d(k_{\text{pred}}, k_{\text{GT}}) \leq \alpha \cdot \max(H, W)$ , where  $d(\cdot)$  denotes Euclidean distance;  $\alpha$  denotes a threshold value;  $H$  and  $W$  denote height and width of the object bounding box or the entire image. Note that as confirmed in [73, 10], using different ground-truth resolutions for evaluation leads to different results, so we set our evaluation on the original resolution.

The results are summarized in Table 1. As shown, IFCAT clearly sets a new state-of-the-art for the three dense semantic correspondence benchmarks. This demonstrates the effectiveness of joint aggregation by outperforming methods that focus on either feature or cost aggregation.

### 5.3 Dense Alignment

We further evaluate our method on the dense alignment dataset HPatches [4]. For each scene, there is a source image and five target images from different viewpoints, along with corresponding ground-truth flows. The resolutions of HPatches range from  $450 \times 600$  to  $1,613 \times 1,210$ . As in [45], we also evaluate on downsampled HPatches [4], where the images are resized to a low resolution ( $240 \times 240$ ). For the evaluation metric, we use the average end-point error (AEPE), computed by averaging the Euclidean distance between the ground-truth and estimated flow, and percentage of correct keypoints (PCK), computed as the ratio of estimated keypoints within a threshold of the ground truth to the total number of keypoints. When evaluating on HPatches [4], following [71, 70] we train our networks on the DPED-CityScape-ADE [71] dataset.



Table 2 summarizes the quantitative results. As shown, IFCAT outperforms existing works by a large margin, clearly achieving state-of-the-art performance. Note that a fair comparison to COTR [32] is not feasible because its use of the zoom-in technique with a multiple inference strategy dramatically boosts its performance as a trade-off to speed. It is shown that RANSAC-Flow [64] and RANSAC-DMP [25] exceeds the performance of our method, but they adopt two-stage inference where the first stage aims to find the homographic transformation between an image pair, which give them an advantage on the HPatches dataset. On its own, IFCAT is demonstrated to be effective, highlighting the importance of integrative aggregation.

## 5.4 Ablation Study

**Aggregation Strategy.** In this ablation study, we compare the performance of different aggregation strategies. Table 3 summarizes the results. There are seven components we evaluate. From **(I)** to **(II)**, we report the results for sole aggregation on either feature or cost volume. We investigate the effectiveness of conditioning features on both images and performing both aggregations in **(III)** and **(IV)**. Lastly, we progressively add the proposed components in **(V)** to **(VII)** to demonstrate their significance. For a fair comparison, we trained all strategies with a single level except for **(VII)**.

As shown, solely aggregating either the feature or cost volume yields limited performance, where **(II)** can be seen as a simplified version of CATs [9]. However, we observe that combining self- and cross-attention, which is highly similar to LoFTR [68], for feature aggregation helps to boost the performance by conditioning features on both images. This highlights the importance of providing information from the other image, which implies that providing a cost volume

that explicitly represents similarity information with respect to each image would help to establish a more accurate correspondence field. Interestingly, **(IV)** shows that performing feature and cost aggregation yields a large performance boost, demonstrating that cost aggregation benefits from powerful feature representations tailored to matching. From **(V)** to **(VII)**, each component contributes appreciably to the improvement of performance, clearly showing the effectiveness of our proposed components. This confirms that, as the result of **(III)** implies, leveraging the complementarity of features and cost volume is of prime importance.

**Depth of Attention Block.** As shown in Fig. 2, we can stack the attention block at each level to increase model capacity and allow further aggregation. In this ablation study, we show the effects of varying the hyperparameter  $N$ . We additionally show comparisons of memory consumption, run time, and number of learnable parameters to indicate their efficiency.

The results are summarized in Table 4. We consistently observe that as the attention block depth increases, the performance is boosted, demonstrating that the earlier aggregations help the subsequent aggregations. We generally observe increasing memory consumption, run-time and number of parameters as  $N$  increases, which are trade-offs to improve performance. Note that during training, the number of parameters has a direct influence on memory consumption, which is a limitation of increasing the attention block depth.

## 6 Conclusion

In this paper, we proposed a novel transformer-based architecture, called Integrative Feature and Cost Aggregation with Transformer (IFCAT), that interleaves feature refinement and cost aggregation by establishing a complementary relationship. Our design based on self- and cross-attention is tailored

Table 3: Aggregation strategies for IFCAT.

Components		SPair-71k $\alpha_{\text{bbox}} = 0.1 \uparrow$	HPatches AEPE $\downarrow$
<b>(I)</b>	Feature self-att.	36.1	84.08
<b>(II)</b>	Cost self-att.	28.7	54.80
<b>(III)</b>	Feature self-att. + cross-att.	38.5	81.72
<b>(IV)</b>	Sequential <b>(III)</b> + cost self-att.	56.5	49.00
<b>(V)</b>	Integrative self-att.	54.7	34.85
<b>(VI)</b>	Integrative self- and cross-att.	58.5	24.41
<b>(VII)</b>	<b>(VI)</b> + hierarchical processing	64.4	17.59

Table 4: Ablations on varying depth of attention block.

# of N	SPair-71k $\alpha_{\text{bbox}} = 0.1 \uparrow$	HPatches AEPE $\downarrow$	Memory [MB]	Runtime [ms]	# of param. [M]
(1,0,0)	55.4	35.02	335.09	35.09	0.58
(2,0,0)	58.5	24.41	354.57	47.23	1.04
(1,1,1)	63.7	20.49	845.06	91.96	0.83
(2,2,2)	64.4	17.59	874.25	138.05	1.55
(3,3,3)	64.7	17.43	903.40	188.43	2.26

for matching and joint enhancement of feature descriptors and the cost volume. This method is formulated in a coarse-to-fine manner, yielding an appreciable performance boost. We have shown that our method surpasses all other existing works on several benchmarks for semantic and geometric matching, establishing new state-of-the-art performance. We also conducted an extensive ablation study to validate our choices.

## References

- [1] Jimmy Lei Ba, Jamie Ryan Kiros, and Geoffrey E Hinton. Layer normalization. *arXiv preprint arXiv:1607.06450*, 2016.
- [2] Dzmitry Bahdanau, Kyunghyun Cho, and Yoshua Bengio. Neural machine translation by jointly learning to align and translate. *arXiv preprint arXiv:1409.0473*, 2014.
- [3] Tim Bailey and Hugh Durrant-Whyte. Simultaneous localization and mapping (slam): Part ii. *IEEE robotics & automation magazine*, 13(3):108–117, 2006.
- [4] Vassileios Balntas, Karel Lenc, Andrea Vedaldi, and Krystian Mikolajczyk. Hpatches: A benchmark and evaluation of handcrafted and learned local descriptors. In *Proceedings of the IEEE conference on computer vision and pattern recognition*, pages 5173–5182, 2017.
- [5] Connelly Barnes, Eli Shechtman, Adam Finkelstein, and Dan B Goldman. Patchmatch: A randomized correspondence algorithm for structural image editing. *ACM Trans. Graph.*, 28(3):24, 2009.
- [6] Herbert Bay, Tinne Tuytelaars, and Luc Van Gool. Surf: Speeded up robust features. In *European conference on computer vision*, pages 404–417. Springer, 2006.
- [7] Michael Calonder, Vincent Lepetit, Christoph Strecha, and Pascal Fua. Brief: Binary robust independent elementary features. In *ECCV*, 2010.
- [8] Minsu Cho, Suha Kwak, Cordelia Schmid, and Jean Ponce. Unsupervised object discovery and localization in the wild: Part-based matching with bottom-up region proposals. In *Proceedings of the IEEE conference on computer vision and pattern recognition*, pages 1201–1210, 2015.
- [9] Seokju Cho, Sunghwan Hong, Sangryul Jeon, Yunsung Lee, Kwanghoon Sohn, and Seungryong Kim. Cats: Cost aggregation transformers for visual correspondence. In *Thirty-Fifth Conference on Neural Information Processing Systems*, 2021.
- [10] Seokju Cho, Sunghwan Hong, and Seungryong Kim. Cats++: Boosting cost aggregation with convolutions and transformers. *arXiv preprint arXiv:2202.06817*, 2022.
- [11] Navneet Dalal and Bill Triggs. Histograms of oriented gradients for human detection. In *CVPR Workshops*, 2005.
- [12] Jia Deng, Wei Dong, Richard Socher, Li-Jia Li, Kai Li, and Li Fei-Fei. Imagenet: A large-scale hierarchical image database. In *2009 IEEE conference on computer vision and pattern recognition*. Ieee, 2009.
- [13] Daniel DeTone, Tomasz Malisiewicz, and Andrew Rabinovich. Superpoint: Self-supervised interest point detection and description. In *Proceedings of the IEEE conference on computer vision and pattern recognition workshops*, pages 224–236, 2018.
- [14] Alexey Dosovitskiy, Lucas Beyer, Alexander Kolesnikov, Dirk Weissenborn, Xiaohua Zhai, Thomas Unterthiner, Mostafa Dehghani, Matthias Minderer, Georg Heigold, Sylvain Gelly, et al. An image is worth 16x16 words: Transformers for image recognition at scale. *arXiv preprint arXiv:2010.11929*, 2020.
- [15] Alexey Dosovitskiy, Philipp Fischer, Eddy Ilg, Philip Hausser, Caner Hazirbas, Vladimir Golkov, Patrick Van Der Smagt, Daniel Cremers, and Thomas Brox. Flownet: Learning optical flow with convolutional networks. In *Proceedings of the IEEE international conference on computer vision*, pages 2758–2766, 2015.
- [16] Mihai Dusmanu, Ignacio Rocco, Tomas Pajdla, Marc Pollefeys, Josef Sivic, Akihiko Torii, and Torsten Sattler. D2-net: A trainable cnn for joint description and detection of local features. In *Proceedings of the IEEE/cvf conference on computer vision and pattern recognition*, pages 8092–8101, 2019.
- [17] Martin A Fischler and Robert C Bolles. Random sample consensus: a paradigm for model fitting with applications to image analysis and automated cartography. *Communications of the ACM*, 24(6):381–395, 1981.

- [18] David Fleet and Yair Weiss. Optical flow estimation. In *Handbook of mathematical models in computer vision*, pages 237–257. Springer, 2006.
- [19] Bumsub Ham, Minsu Cho, Cordelia Schmid, and Jean Ponce. Proposal flow. In *CVPR*, 2016.
- [20] Bumsub Ham, Minsu Cho, Cordelia Schmid, and Jean Ponce. Proposal flow: Semantic correspondences from object proposals. *IEEE transactions on pattern analysis and machine intelligence*, 2017.
- [21] Kaiming He, Christoph Rhemann, Carsten Rother, Xiaoou Tang, and Jian Sun. A global sampling method for alpha matting. In *CVPR 2011*, pages 2049–2056. IEEE, 2011.
- [22] Kaiming He, Xiangyu Zhang, Shaoqing Ren, and Jian Sun. Deep residual learning for image recognition. In *Proceedings of the IEEE conference on computer vision and pattern recognition*, 2016.
- [23] Sunghwan Hong, Seokju Cho, Jisu Nam, and Seungryong Kim. Cost aggregation is all you need for few-shot segmentation. *arXiv preprint arXiv:2112.11685*, 2021.
- [24] Sunghwan Hong, Seokju Cho, Jisu Nam, Stephen Lin, and Seungryong Kim. Cost aggregation with 4d convolutional swin transformer for few-shot segmentation. *arXiv preprint arXiv:2207.10866*, 2022.
- [25] Sunghwan Hong and Seungryong Kim. Deep matching prior: Test-time optimization for dense correspondence. In *Proceedings of the IEEE/CVF International Conference on Computer Vision (ICCV)*, 2021.
- [26] Asmaa Hosni, Christoph Rhemann, Michael Bleyer, Carsten Rother, and Margrit Gelautz. Fast cost-volume filtering for visual correspondence and beyond. *PAMI*, 2012.
- [27] Shuaiyi Huang, Qiuyue Wang, Songyang Zhang, Shipeng Yan, and Xuming He. Dynamic context correspondence network for semantic alignment. In *ICCV*, 2019.
- [28] Zhaoyang Huang, Xiaoyu Shi, Chao Zhang, Qiang Wang, Ka Chun Cheung, Hongwei Qin, Jifeng Dai, and Hongsheng Li. Flowformer: A transformer architecture for optical flow. *arXiv preprint arXiv:2203.16194*, 2022.
- [29] Tak-Wai Hui, Xiaoou Tang, and Chen Change Loy. Liteflownet: A lightweight convolutional neural network for optical flow estimation. In *Proceedings of the IEEE conference on computer vision and pattern recognition*, pages 8981–8989, 2018.
- [30] Sangryul Jeon, Seungryong Kim, Dongbo Min, and Kwanghoon Sohn. Parn: Pyramidal affine regression networks for dense semantic correspondence. In *Proceedings of the European Conference on Computer Vision (ECCV)*, pages 351–366, 2018.
- [31] Sangryul Jeon, Dongbo Min, Seungryong Kim, Jihwan Choe, and Kwanghoon Sohn. Guided semantic flow. In *ECCV*. Springer, 2020.
- [32] Wei Jiang, Eduard Trulls, Jan Hosang, Andrea Tagliasacchi, and Kwang Moo Yi. Cotr: Correspondence transformer for matching across images. In *Proceedings of the IEEE/CVF International Conference on Computer Vision*, pages 6207–6217, 2021.
- [33] Angelos Katharopoulos, Apoorv Vyas, Nikolaos Pappas, and François Fleuret. Transformers are rnns: Fast autoregressive transformers with linear attention. In *International Conference on Machine Learning*, pages 5156–5165. PMLR, 2020.
- [34] Seungryong Kim, Stephen Lin, Sang Ryul Jeon, Dongbo Min, and Kwanghoon Sohn. Recurrent transformer networks for semantic correspondence. *Advances in neural information processing systems*, 31, 2018.
- [35] Jae Yong Lee, Joseph DeGol, Victor Fragoso, and Sudipta N Sinha. Patchmatch-based neighborhood consensus for semantic correspondence. In *Proceedings of the IEEE/CVF Conference on Computer Vision and Pattern Recognition*, pages 13153–13163, 2021.
- [36] Junghyup Lee, Dohyung Kim, Jean Ponce, and Bumsub Ham. Sfnets: Learning object-aware semantic correspondence. In *CVPR*, 2019.
- [37] Shuda Li, Kai Han, Theo W Costain, Henry Howard-Jenkins, and Victor Prisacariu. Correspondence networks with adaptive neighbourhood consensus. In *Proceedings of the IEEE/CVF Conference on Computer Vision and Pattern Recognition*, pages 10196–10205, 2020.
- [38] Xin Li, Deng-Ping Fan, Fan Yang, Ao Luo, Hong Cheng, and Zicheng Liu. Probabilistic model distillation for semantic correspondence. In *Proceedings of the IEEE/CVF Conference on Computer Vision and Pattern Recognition*, pages 7505–7514, 2021.

- [39] Ce Liu, Jenny Yuen, and Antonio Torralba. Sift flow: Dense correspondence across scenes and its applications. *IEEE transactions on pattern analysis and machine intelligence*, 33(5):978–994, 2010.
- [40] Yanbin Liu, Linchao Zhu, Makoto Yamada, and Yi Yang. Semantic correspondence as an optimal transport problem. In *Proceedings of the IEEE/CVF Conference on Computer Vision and Pattern Recognition*, 2020.
- [41] Ze Liu, Yutong Lin, Yue Cao, Han Hu, Yixuan Wei, Zheng Zhang, Stephen Lin, and Baining Guo. Swin transformer: Hierarchical vision transformer using shifted windows. *arXiv preprint arXiv:2103.14030*, 2021.
- [42] Ilya Loshchilov and Frank Hutter. Decoupled weight decay regularization. *arXiv preprint arXiv:1711.05101*, 2017.
- [43] David G Lowe. Distinctive image features from scale-invariant keypoints. *International journal of computer vision*, 60(2):91–110, 2004.
- [44] Jiachen Lu, Jinghan Yao, Junge Zhang, Xiatian Zhu, Hang Xu, Weiguo Gao, Chunjing Xu, Tao Xiang, and Li Zhang. Soft: Softmax-free transformer with linear complexity. *arXiv preprint arXiv:2110.11945*, 2021.
- [45] Iaroslav Melekhov, Aleksei Tulpin, Torsten Sattler, Marc Pollefeys, Esa Rahtu, and Juho Kannala. Dgc-net: Dense geometric correspondence network. In *WACV*, 2019.
- [46] Juhong Min, Seungwook Kim, and Minsu Cho. Convolutional hough matching networks for robust and efficient visual correspondence. *arXiv preprint arXiv:2109.05221*, 2021.
- [47] Juhong Min, Seungwook Kim, and Minsu Cho. Convolutional hough matching networks for robust and efficient visual correspondence. *arXiv preprint arXiv:2109.05221*, 2021.
- [48] Juhong Min, Jongmin Lee, Jean Ponce, and Minsu Cho. Hyperpixel flow: Semantic correspondence with multi-layer neural features. In *Proceedings of the IEEE/CVF International Conference on Computer Vision*, 2019.
- [49] Juhong Min, Jongmin Lee, Jean Ponce, and Minsu Cho. Spair-71k: A large-scale benchmark for semantic correspondence. *arXiv preprint arXiv:1908.10543*, 2019.
- [50] Juhong Min, Jongmin Lee, Jean Ponce, and Minsu Cho. Learning to compose hypercolumns for visual correspondence. In *Computer Vision—ECCV 2020: 16th European Conference, Glasgow, UK, August 23–28, 2020, Proceedings, Part XV 16*. Springer, 2020.
- [51] Yuki Ono, Eduard Trulls, Pascal Fua, and Kwang Moo Yi. Lf-net: Learning local features from images. *Advances in neural information processing systems*, 31, 2018.
- [52] Adam Paszke, Sam Gross, Soumith Chintala, Gregory Chanan, Edward Yang, Zachary DeVito, Zeming Lin, Alban Desmaison, Luca Antiga, and Adam Lerer. Automatic differentiation in pytorch. 2017.
- [53] William Peebles, Jun-Yan Zhu, Richard Zhang, Antonio Torralba, Alexei Efros, and Eli Shechtman. Gan-supervised dense visual alignment. *arXiv preprint arXiv:2112.05143*, 2021.
- [54] James Philbin, Ondrej Chum, Michael Isard, Josef Sivic, and Andrew Zisserman. Object retrieval with large vocabularies and fast spatial matching. In *CVPR*. IEEE, 2007.
- [55] Jerome Revaud, Philippe Weinzaepfel, César De Souza, Noe Pion, Gabriela Csurka, Yohann Cabon, and Martin Humenberger. R2d2: repeatable and reliable detector and descriptor. *arXiv preprint arXiv:1906.06195*, 2019.
- [56] Ignacio Rocco, Relja Arandjelovic, and Josef Sivic. Convolutional neural network architecture for geometric matching. In *CVPR*, 2017.
- [57] Ignacio Rocco, Relja Arandjelović, and Josef Sivic. End-to-end weakly-supervised semantic alignment. In *CVPR*, 2018.
- [58] Ignacio Rocco, Relja Arandjelović, and Josef Sivic. Efficient neighbourhood consensus networks via submanifold sparse convolutions. In *ECCV*, 2020.
- [59] Ignacio Rocco, Mircea Cimpoi, Relja Arandjelović, Akihiko Torii, Tomas Pajdla, and Josef Sivic. Neighbourhood consensus networks. *arXiv preprint arXiv:1810.10510*, 2018.
- [60] Paul-Edouard Sarlin, Daniel DeTone, Tomasz Malisiewicz, and Andrew Rabinovich. Superglue: Learning feature matching with graph neural networks. In *CVPR*, 2020.

- [61] Daniel Scharstein and Richard Szeliski. A taxonomy and evaluation of dense two-frame stereo correspondence algorithms. *International journal of computer vision*, 2002.
- [62] Johannes L Schonberger and Jan-Michael Frahm. Structure-from-motion revisited. In *Proceedings of the IEEE conference on computer vision and pattern recognition*, pages 4104–4113, 2016.
- [63] Paul Hongsuck Seo, Jongmin Lee, Deunsol Jung, Bohyung Han, and Minsu Cho. Attentive semantic alignment with offset-aware correlation kernels. In *Proceedings of the European Conference on Computer Vision (ECCV)*, pages 349–364, 2018.
- [64] Xi Shen, François Darmon, Alexei A Efros, and Mathieu Aubry. Ransac-flow: generic two-stage image alignment. In *European Conference on Computer Vision*, pages 618–637. Springer, 2020.
- [65] Karen Simonyan and Andrew Zisserman. Very deep convolutional networks for large-scale image recognition. *arXiv preprint arXiv:1409.1556*, 2014.
- [66] Richard Sinkhorn. Diagonal equivalence to matrices with prescribed row and column sums. *The American Mathematical Monthly*, 1967.
- [67] Deqing Sun, Xiaodong Yang, Ming-Yu Liu, and Jan Kautz. Pwc-net: Cnns for optical flow using pyramid, warping, and cost volume. In *CVPR*, 2018.
- [68] Jiaming Sun, Zehong Shen, Yuang Wang, Hujun Bao, and Xiaowei Zhou. Loftr: Detector-free local feature matching with transformers. In *Proceedings of the IEEE/CVF conference on computer vision and pattern recognition*, pages 8922–8931, 2021.
- [69] Engin Tola, Vincent Lepetit, and Pascal Fua. Daisy: An efficient dense descriptor applied to wide-baseline stereo. *IEEE transactions on pattern analysis and machine intelligence*, 32(5):815–830, 2009.
- [70] Prune Truong, Martin Danelljan, Luc V Gool, and Radu Timofte. Gocor: Bringing globally optimized correspondence volumes into your neural network. *Advances in Neural Information Processing Systems*, 33:14278–14290, 2020.
- [71] Prune Truong, Martin Danelljan, and Radu Timofte. Glu-net: Global-local universal network for dense flow and correspondences. In *Proceedings of the IEEE/CVF conference on computer vision and pattern recognition*, pages 6258–6268, 2020.
- [72] Prune Truong, Martin Danelljan, Luc Van Gool, and Radu Timofte. Learning accurate dense correspondences and when to trust them. In *Proceedings of the IEEE/CVF Conference on Computer Vision and Pattern Recognition*, 2021.
- [73] Prune Truong, Martin Danelljan, Fisher Yu, and Luc Van Gool. Probabilistic warp consistency for weakly-supervised semantic correspondences. *arXiv preprint arXiv:2203.04279*, 2022.
- [74] Ashish Vaswani, Noam Shazeer, Niki Parmar, Jakob Uszkoreit, Llion Jones, Aidan N Gomez, Łukasz Kaiser, and Illia Polosukhin. Attention is all you need. In *Advances in neural information processing systems*, 2017.
- [75] Sinong Wang, Belinda Z Li, Madian Khabsa, Han Fang, and Hao Ma. Linformer: Self-attention with linear complexity. *arXiv preprint arXiv:2006.04768*, 2020.
- [76] Chuhan Wu, Fangzhao Wu, Tao Qi, Yongfeng Huang, and Xing Xie. Fastformer: Additive attention can be all you need. *arXiv preprint arXiv:2108.09084*, 2021.
- [77] Haofei Xu, Jing Zhang, Jianfei Cai, Hamid Rezaatofighi, and Dacheng Tao. Gmflow: Learning optical flow via global matching. *arXiv preprint arXiv:2111.13680*, 2021.
- [78] Gengshan Yang and Deva Ramanan. Volumetric correspondence networks for optical flow. *Advances in neural information processing systems*, 32, 2019.
- [79] Kwang Moo Yi, Eduard Trulls, Vincent Lepetit, and Pascal Fua. Lift: Learned invariant feature transform. In *ECCV*, 2016.
- [80] Kuk-Jin Yoon and In So Kweon. Adaptive support-weight approach for correspondence search. *IEEE transactions on pattern analysis and machine intelligence*, 28(4):650–656, 2006.
- [81] Dongyang Zhao, Ziyang Song, Zhenghao Ji, Gangming Zhao, Weifeng Ge, and Yizhou Yu. Multi-scale matching networks for semantic correspondence. In *Proceedings of the IEEE/CVF International Conference on Computer Vision*, pages 3354–3364, 2021.
- [82] Zihua Zheng, Ni Nie, Zhi Ling, Pengfei Xiong, Jiangyu Liu, Hao Wang, and Jiankun Li. Dip: Deep inverse patchmatch for high-resolution optical flow. *arXiv preprint arXiv:2204.00330*, 2022.

## Appendix

In this document, we provide more implementation details and psuedo-code of IFCAT, and more results on SPair-71k [49], PF-PASCAL [20], PF-WILLOW [19] and HPatches [4].

### More Details

**Training Details.** For training, we employ the same augmentation strategy introduced in [9]. To implement 4D convolutions, we use separable 4D convolutions for efficient computation, which is introduced in VCN [78]. All separable 4D convolutions are followed by ReLU activation and Layer Normalization [1]. We set the weight decay to 0.05 and the learning rate to  $1e^{-4}$  for IFCAT and to  $1e^{-6}$  for the backbone, which is halved at epochs 30 and 40.

**Psuedo-code.** We present Pytorch-like Psuedo-code of the proposed method in Alg. 1.

**More Qualitative Results.** We provide more qualitative results for SPair-71k [49] in Fig. 1, PF-PASCAL [20] in Fig. 2, PF-WILLOW [20] in Fig. 3, and HPatches [4] in Fig. 4. We also present more visualization of the attention maps in Fig. 5.

### Limitations

An apparent limitation of the proposed method is that as IFCAT acts on the cost volume, it is not feasible to perform cost aggregation at higher resolutions. The maximum resolution that would be accessible to users is  $64^4$ . This makes the use of standard transformer for attention computation infeasible in terms of memory consumption. Another limitation may be when given a pair of images that are not relevant or show completely different objects, such that there are no correspondences between views, the proposed method lacks an ability to prevent establishing correspondences.

### Broader Impact

Our network can be beneficial in a wide range of applications, including simultaneous localization and mapping (SLAM) [3], augmented reality (AR) [53], object tracking, structure from motion (SfM) [62], optical flow [18], and image editing [5, 34]. As a future work, we could apply the proposed method to different tasks, including feature matching, segmentation and optical flow. Our work would not pose significantly malicious threats on its own.

---

**Algorithm 1** Pseudo-Code, PyTorch-like

---

```
class TransformerLayer:
    def forward(corr, src_feat, trg_feat):
        corr_src, src_feat_refined = integrative_self_attention(corr, src_feat)
        corr_trg, trg_feat_refined = integrative_self_attention(transpose(corr), trg_feat)

        corr = corr_src + transpose(corr_trg)
        corr = corr + conv4d_1(cost_computation(src_feat_refined, trg_feat_refined))
        corr = corr + conv4d_2(corr)

        src_feat_refined, trg_feat_refined = integrative_cross_attention(corr, src_feat_refined,
            trg_feat_refined)

        corr = corr + conv4d_3(cost_computation(src_feat_refined, trg_feat_refined))
        corr = corr + conv4d_4(corr)

    return corr, src_feat_refined, trg_feat_refined

class IFCAT:
    def forward(trg_img, src_img):
        src_feat_list = feature_backbone(src_img)
        trg_feat_list = feature_backbone(trg_img)
        src_feats = projection(src_feat_list)
        trg_feats = projection(trg_feat_list)

        correlations = []

        corr_1 = correlation(src_feat_list[0], src_feat_list[0])
        corr_1 = conv4d_1(corr_1)
        src_feat_1, trg_feat_1 = src_feats[0], trg_feats[0]
        corr_1, src_feat_1, trg_feat_1 = transformer_layer[0](corr_1, src_feat_1, trg_feat_1)
        correlations.append(cost_computation(src_feat_1, trg_feat_1))

        corr_2 = correlation(src_feat_list[1], src_feat_list[1])
        corr_2 = corr_1 + conv4d_2(corr_2)

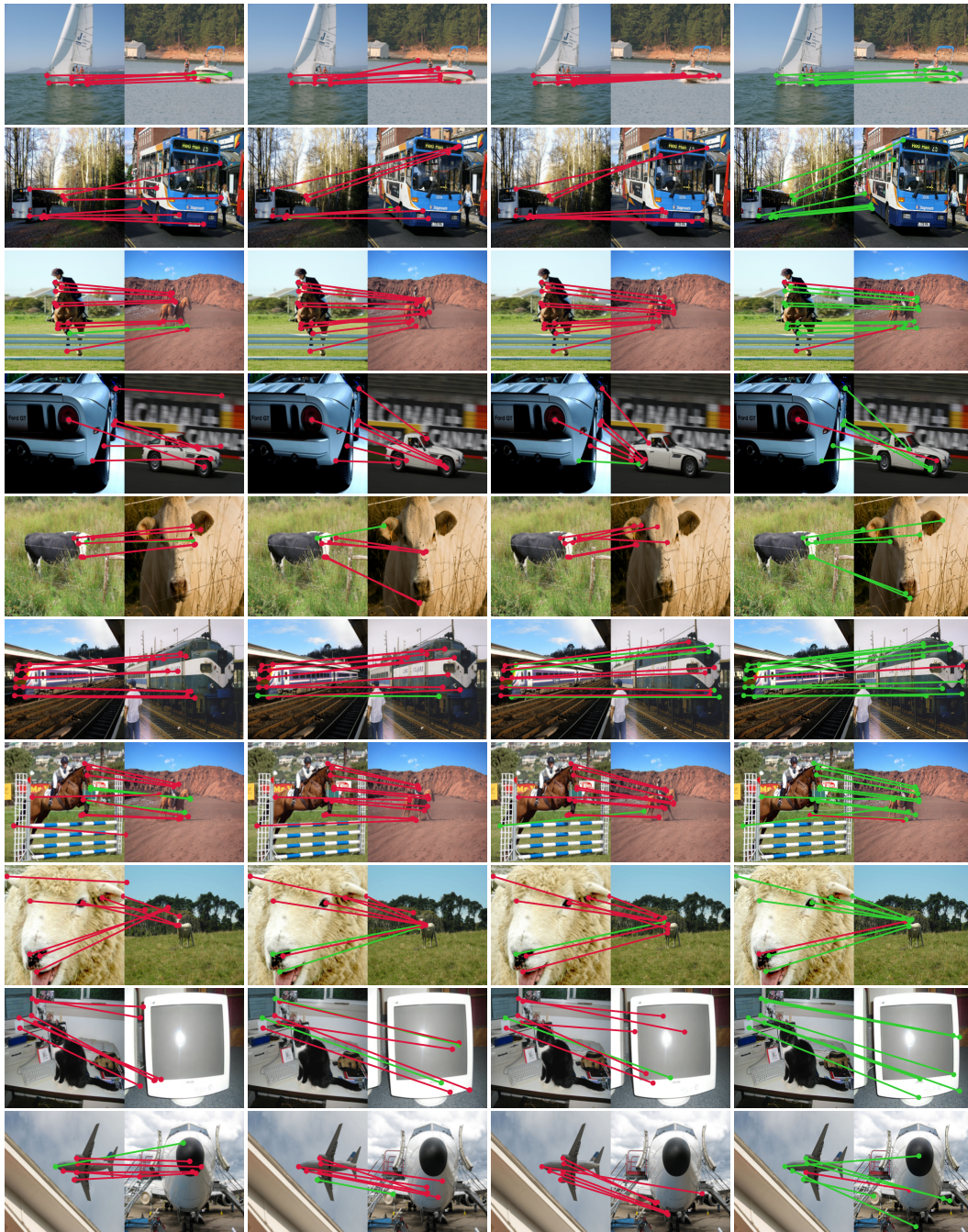
        src_feat_2 = interpolate(linear_1(src_feat_1), scale_factor=2) + src_feats[1]
        trg_feat_2 = interpolate(linear_1(trg_feat_1), scale_factor=2) + trg_feats[1]
        corr_2, src_feat_2, trg_feat_2 = transformer_layer[1](corr_2, src_feat_2, trg_feat_2)
        correlations.append(cost_computation(src_feat_2, trg_feat_2))

        corr_3 = correlation(src_feat_list[2], src_feat_list[2])
        corr_3 = corr_2 + conv4d_3(corr_3)

        src_feat_3 = interpolate(linear_2(src_feat_2), scale_factor=2) + src_feats[2]
        trg_feat_3 = interpolate(linear_2(trg_feat_2), scale_factor=2) + trg_feats[2]
        corr_3, src_feat_3, trg_feat_3 = transformer_layer[2](corr_3, src_feat_3, trg_feat_3)
        correlations.append(cost_computation(src_feat_3, trg_feat_3))

        corr_upsampled = [interpolate4d(x, (64, 64, 64, 64)) for x in correlations]
        c_star = sum(corr_upsampled) / len(corr_upsampled)
    return flow_estimation(c_star)
```

---



(a) DHPF [50]

(b) CHM [46]

(c) CATs [9]

(d) IFCAT

Figure 1: **Qualitative results on SPair-71k [49]:** keypoints transfer results by (a) DHPF [50], (b) CHM [46], and (c) CATs [9], and (d) ours. Note that green and red lines denote correct and wrong predictions, respectively, with respect to the ground-truth.



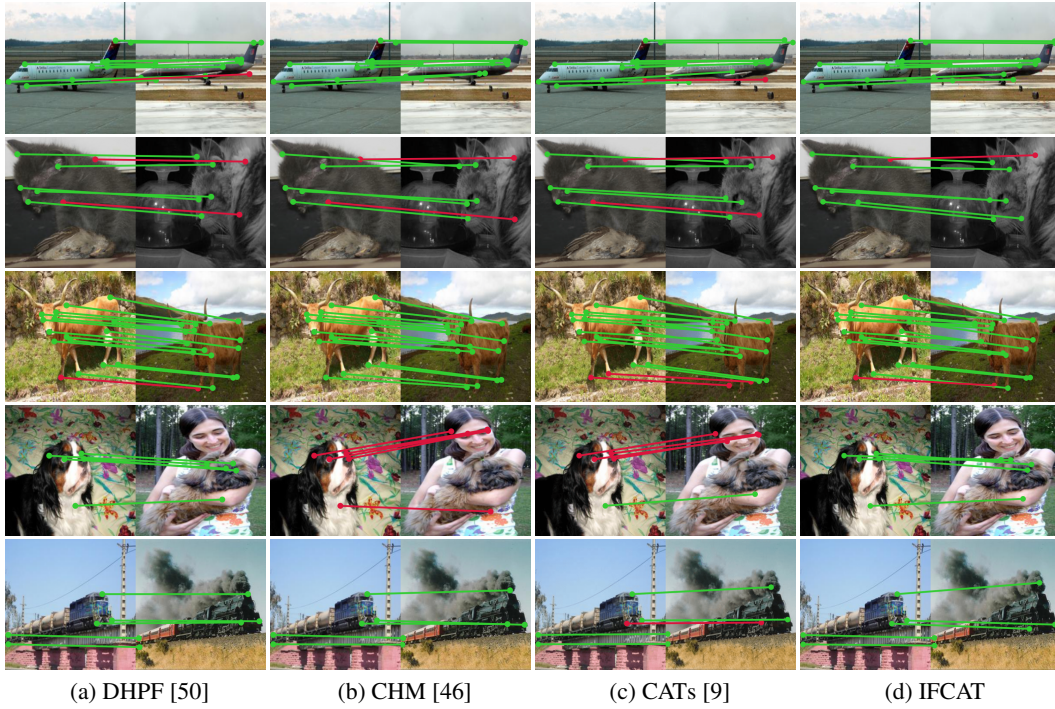


Figure 2: **Qualitative results on PF-PASCAL [20]**

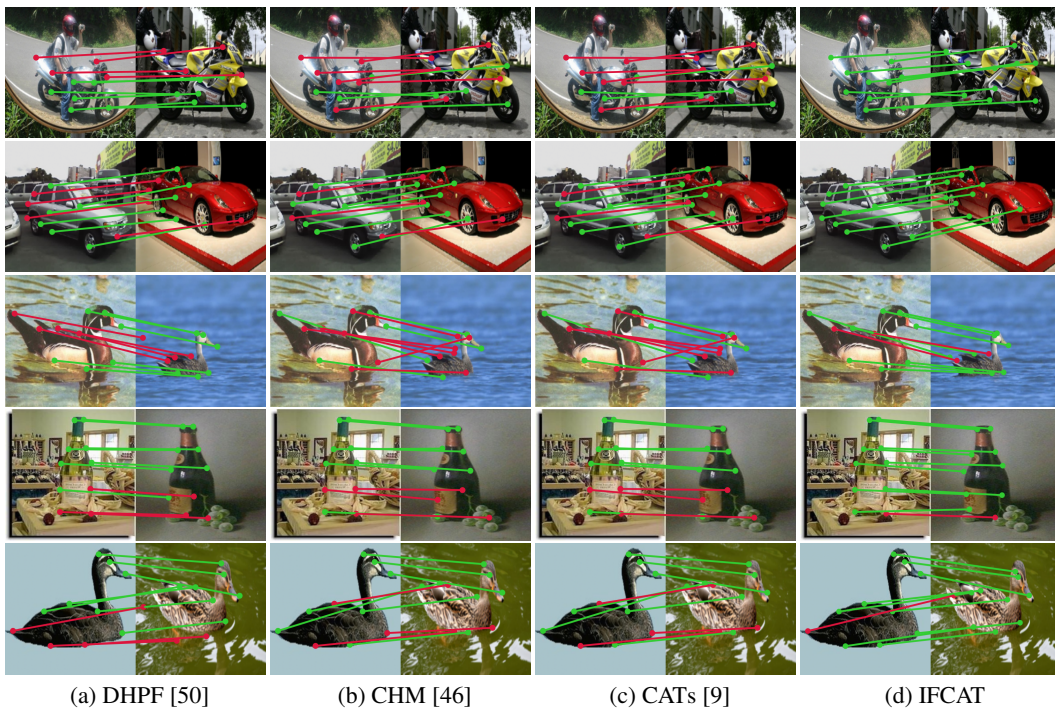


Figure 3: **Qualitative results on PF-WILLOW [19].**



Source

Target

GT

Prediction

Figure 4: Qualitative results on HPatches [4].

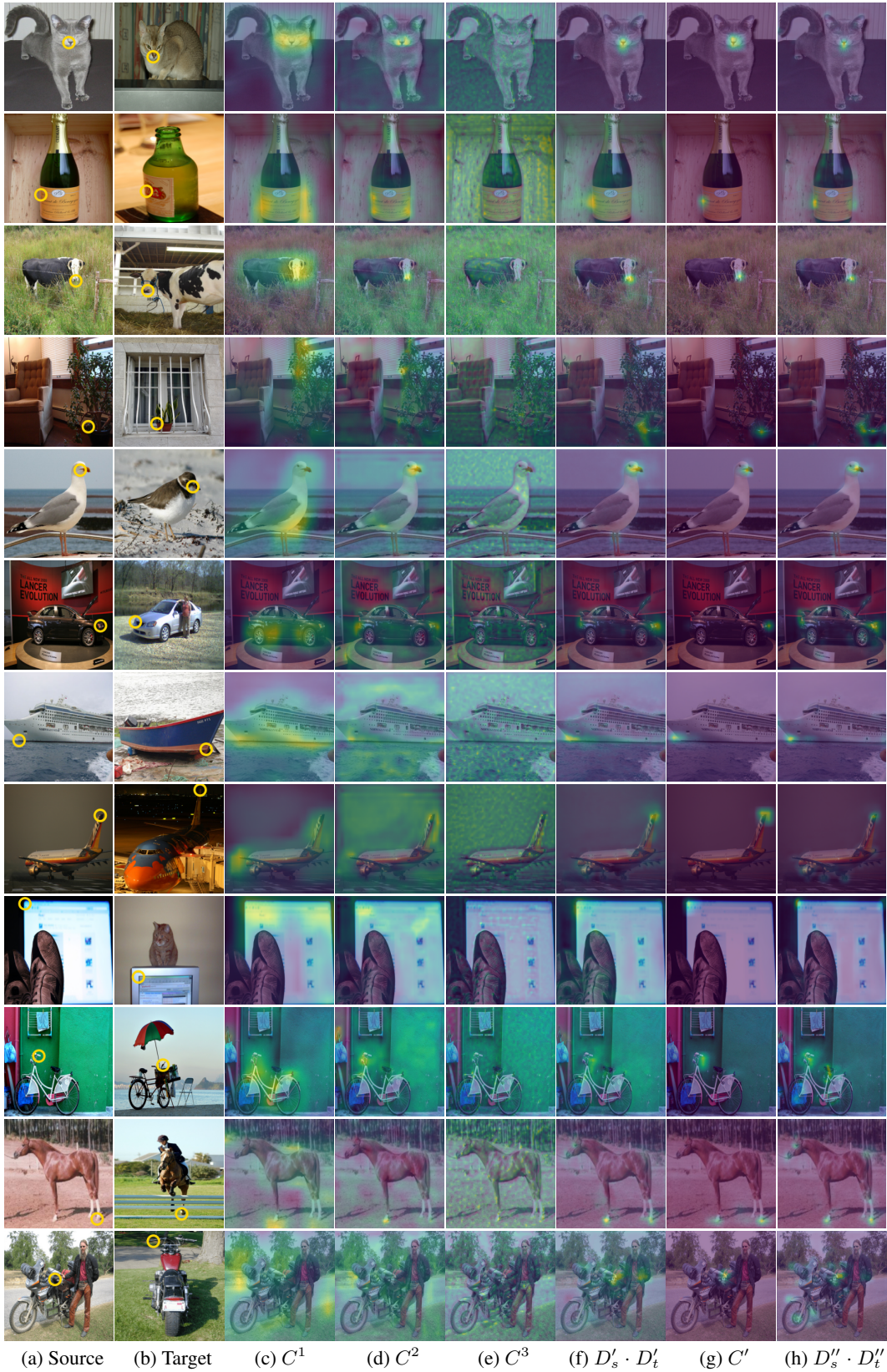


Figure 5: Visualization of attention maps.